

Optical and transport properties of heavy fermions: theory compared to experiment.

N S Vidhyadhiraja and David E Logan

University of Oxford, Physical and Theoretical Chemistry Laboratory,
South Parks Rd, Oxford OX1 3QZ, UK

Abstract.

Employing a local moment approach to the periodic Anderson model within the framework of dynamical mean-field theory, direct comparison is made between theory and experiment for the d.c. transport and optical conductivities of paramagnetic heavy fermion and intermediate valence metals. Four materials, exhibiting a diverse range of behaviour in their transport/optics, are analysed in detail: CeB_6 , YbAl_3 , CeAl_3 and CeCoIn_5 . Good agreement between theory and experiment is in general found, even quantitatively, and a mutually consistent picture of transport and optics results.

PACS numbers: 71.27.+a Strongly correlated electron systems; heavy fermions – 75.20.Hr Local moment in compounds and alloys; Kondo effect, valence fluctuations, heavy fermions

Submitted to: J. Phys.: Condens. Matter

1. Introduction.

Heavy electron materials have long been the subject of extensive investigation, for reviews see e.g. [1–7]. Yet in many respects even their normal paramagnetic phase, be it metallic or insulating, has eluded a unified microscopic description on all experimentally relevant temperature (T) and/or frequency (ω) scales. The canonical theoretical model here is of course the periodic Anderson model (PAM). Within the general framework of dynamical mean-field theory [8–11] we have developed in the preceding paper [12] (here referred to as I) a non-perturbative local moment approach to paramagnetic metallic phases of the PAM, with a focus on d.c. transport and optics; following earlier work on $T = 0$ dynamics [13] and on Kondo insulators [14, 15]. The primary emphasis of I is the Kondo lattice regime relevant to strong correlated heavy fermion (HF) metals. Dynamics/transport on all relevant ($\omega; T$)-scales are encompassed, from the low-energy behaviour characteristic of the lattice coherent Fermi liquid, through incoherent effective single-impurity physics to non-universal high-energy scales. The underlying theory is not however restricted to the Kondo lattice regime, enabling it also to handle e.g. intermediate valence (IV) behaviour.

The present paper is an attempt to provide at least a partial answer to the question: to what extent are the optical and d.c. transport properties of HF and related materials captured by the PAM and our theory for it? That clearly requires direct, quantitative comparison between theory and experiment, which is our purpose here. Specifically, we consider in detail the transport and optics of four materials: CeB_6 , YbAl_3 , CeAl_3 and CeCoIn_5 , all HF metals with the exception of the IV compound YbAl_3 , and exhibiting a diverse range of behaviour in their transport and optical behaviour. The materials are analysed on a case by case basis in xs 3-6, following a discussion (x2) of relevant issues involved in making the comparison; and we believe it fair to claim that the theory provides a striking account of experiment.

2. Background issues

The Hamiltonian for the PAM is given by equation (2.1) of I, and its physical content is simple: a single correlated f-level in each unit cell hybridizes locally to an uncorrelated conduction band. The model is moreover specified by only four bare/material parameters rendering it minimalist in terms of comparison to experiment — the more so when one recalls that it encompasses regimes of behaviour as diverse as strongly correlated heavy fermion metals and Kondo insulators, intermediate valence, and weak coupling. The dimensionless bare parameters are U , V , ϵ_c and ϵ_f (in units of the conduction electron hopping, $t \approx 1$), with U denoting the local f-level interaction strength and V the local one-electron hybridization coupling an f-level to the conduction band. The energy of the local conduction orbital, ϵ_c , determines the centre of gravity of the free conduction band relative to the Fermi level (and thereby the conduction band filling, n_c); and ϵ_f denotes the f-orbital energy. An equivalent parameter set is U , V , ϵ_c and ϵ_f , where $\epsilon_f = 1 + 2\epsilon_f = U$ specifies the f-level asymmetry.

The non-interacting limit of the model ($U = 0$) is certainly trivial. But in that case — for all T — the d.c. resistivity of the metallic state vanishes, and the optical conductivity contains no absorption below the direct gap save for a δ -function Drude contribution at $\omega = 0$, see I. That this behaviour bears scant comparison to experiment reflects the fact that the essential physics is driven by scattering due to electron interactions. It is of course the latter, and the resultant many-body nature of the problem, that renders the PAM non-trivial.

In considering d.c. transport, the first requirement in comparing theory to experiment is thus to extract the contribution ($\rho_{\text{mag}}^{\text{exp}}(T)$) to the measured resistivity ($\rho(T)$) that isolates the interaction contributions from those of phonons and static impurity scattering. This is given, ideally, by

$$\rho_{\text{mag}}^{\text{exp}}(T) = \rho(T) - \rho(0) - \rho_{\text{ph}}(T):$$

The first term removes the residual ($T = 0$) resistivity, and hence impurity scattering contribution on the assumption that the latter is T -independent. The second removes the contribution from phonons; usually taken in practice (as assumed in the following)

to be the resistivity of the non-magnetic homologue compound with the magnetic ion Ce (or Yb) replaced by La (or Lu), on the assumption that interactions in the latter are negligible. For most systems the phonon contribution is generally negligible for $T \gtrsim 50\text{K}$ or so.

While this prescription is straightforward in principle, we first deal with a complication that can arise in practice. Experimentally it is the resistance that is measured directly. To convert to a sample independent resistivity requires spatial dimensions to be known with reasonable precision. That does not pose a problem with large crystals, but may do for small samples. Examples arise in the literature where reported $\rho(T)$'s from different groups differ quite significantly; we encounter one such in the case of CeCoIn_5 considered in §6. Absolute resistivities would thus be related to measured values by e.g. $\rho^0(T)$ and $\rho^{\text{ph}}(T)$, where ρ^0 and ρ^{ph} denote experimental 'intrinsic' factors. For comparison to theory (equation (2.2) below) we require however only the relative factors ρ^0/ρ^{ph} , to which end we replace the above by

$$\rho_{\text{mag}}^{\text{exp}}(T) = a \rho(T) \quad (0)g_{\text{ph}}(T) \quad (2.1)$$

where $a = 1$ in the ideal case (the majority of systems considered below).

The experimental $\rho_{\text{mag}}^{\text{exp}}(T)$ is to be compared to $\rho_{\text{mag}}(T)$ arising from the theory of I for the PAM (where ρ_{mag} was denoted simply by ρ). The system is generically characterized by a low-energy coherence scale $\xi_L = ZV^2$, with Z the quasiparticle weight or inverse mass renormalization factor. This scale is a complicated function of the underlying bare parameters, see e.g. [13] and refs therein. But in the strong coupling Kondo lattice regime ξ_L is exponentially small (because Z is). In consequence, $\rho_{\text{mag}}(T)$ exhibits scaling in terms of ξ_L , i.e. is of form

$$\rho_{\text{mag}}(T) = H \frac{T}{\xi_L} \quad (2.2)$$

with the temperature dependence encoded in T/ξ_L , independent of the interaction strength U and hybridization V (H is a trivial overall scale factor, $H=1$ in the notation of I); the scaling holding for (any) fixed ξ_c and ξ_L . The scaling resistivity is moreover only weakly dependent on ξ_c , and for $T/\xi_L \ll 1$ or so is in fact independent of ξ_c , reflecting the crossover to incoherent effective single impurity physics (as detailed in I, see e.g. figure 8). This enables direct connection to experiment, via the extent to which the scaling form equation (2.2) captures the T -dependence of experimental resistivities; and indeed also their pressure dependence, for although ξ_L will change with pressure the scaling behaviour should remain intact (we consider this explicitly in the case of CeAl_3 , §5). Success in this regard also enables ξ_L to be determined directly, there being no hope of calculating it 'ab initio' with any meaningful accuracy. Finally, we add that comparison of theory/experiment proceeds along the same lines away from the asymptotic Kondo lattice regime, in dealing e.g. with intermediate valence materials or intermediate/weak coupling compounds. Here a full parameter set ξ_c , ξ_L , U and V must in general be specified; but $\rho_{\text{mag}}(T)$ can always be cast in the form equation (2.2), and appropriate comparison can be made.

Although our comments above focus on static transport, a central purpose of the paper is also to make direct comparison between experiment and theory for optics, on all experimentally relevant frequency and temperature scales. Given prior analysis of d.c. transport, the underlying model/material parameters are known, either wholly or in part. There is then little room for manoeuvre; the resultant theory either captures the optical behaviour or not, providing a further and quite stringent test of the model's material applicability.

The main physical effect omitted in the PAM itself is that of crystal electric fields (CEFs). The atomic levels of e.g. Ce^{3+} , $^2\text{F}_{5/2}$, are generically split into three doublets, the excited levels lying above the ground state by ϵ_1, ϵ_2 . For sufficiently low T only the lowest level matters, it being this alone the PAM seeks to capture. Although the material specific ϵ_i are usually larger than $k_B T_L$ (itself typically $\sim 10-100\text{K}$), they often lie in the interval $\sim 300\text{K}$. Their qualitative influence on d.c. transport is clear, for additional conduction channels are opened up in accessing higher CEF levels with increasing T . Quantitatively however, the effect is hard to gauge a priori, its magnitude naturally depending on how effectively the higher CEF levels couple to the conduction band. Where present and effective, we can expect to see it as a decrease in the experimental resistivity below that predicted by the 1-channel PAM, the onset of the deviation appearing at $T \sim \epsilon_1$. We add here that while the role of CEF effects has been studied in the context of single-impurity Anderson/Kondo models [16{20], with application to lattice-based systems for sufficiently high temperatures where lattice coherence can be neglected, we are not aware of corresponding work in the context of lattice-fermion models.

Finally, we note that our comparison of theory/experiment for Kondo insulators in [15] was free from most of the considerations above. There, theory was compared directly to the experimental $\rho(T)$, for several reasons. First, in contrast to the case of heavy fermion metals, resistivities of the non-magnetic homologues are sufficiently small compared to those of the Kondo insulating material that $\rho_{ph}(T)$ in equation (2.1) can be neglected with impunity. That in turn means that any sample geometry factor $a \neq 1$ in equation (2.1) can simply be absorbed into the overall scale factor (equation (2.2)), so any lack of precision in obtaining $\rho(T)$ is immaterial. The role of impurities is also different in Kondo insulators. In metals this arises from static impurity scattering, presumed to be T -independent and generating the finite residual resistivity $\rho(0)$; which is thus subtracted out as in equation (2.1). In Kondo insulators by contrast $\rho(T)$ diverges as $T \rightarrow 0$, reflecting the insulating ground state. This occurs even in the presence of localized impurity states in the $T = 0$ insulating gap; which generate conduction by variable-range hopping, generally operative over a narrow T -interval (e.g. $\sim 8\text{K}$ for SmB_6 [15,21]), and whose net effect on $\rho(T)$ at temperatures above this interval (where direct comparison is made to experiment) is usually sufficiently small to be neglected.

We turn now to comparison with experiment for the metallic heavy fermion and intermediate valence materials considered.

3. CeB₆

Among the rare-earth hexaborides, the Kondo insulator SmB₆ and the heavy fermion compound CeB₆ have been investigated for many years [1, 7, 22–26]. The former was considered in our recent work [15] on the particle-hole symmetric PAM. There it was shown that a single low-energy (indirect gap) scale underlies the temperature dependence of both the static and optical conductivity, and (with minimal input of bare material parameters) the frequency dependence of the optics as well. Here we consider its metallic counterpart CeB₆, likewise a cubic system [22]. At the lowest temperatures, various antiferromagnetic phase transitions occur between $T = 1.6 - 3.3\text{K}$ [22, 24, 26]; above (and below) which the paramagnetic phase arises, Phase-I' for $T > 3.3\text{K}$.

The relative ease with which large, clean single crystals of CeB₆ can be grown (see e.g. [26]) has been a motivating factor in its investigation. The d.c. resistivity has been measured by several groups (e.g. [22, 26]) and since the sample quality is in general good, the residual resistivity is very small. In addition, the relatively large crystal sizes imply small errors in sample geometry, hence the factor a in equations (2.1) can safely be assumed to be 1. The phonon contribution to the resistivity is as usual taken as the resistivity of the non-magnetic homologue LaB₆ [22], the latter having the same lattice structure with similar lattice parameters and phonon dispersion as CeB₆ (from inelastic neutron scattering [22]). The experimental magnetic resistivity $\rho_{\text{mag}}^{\text{exp}}(T)$ is then readily obtained [22], and shown in figure 1 (we add that the phonon contribution kicks in only for $T \gtrsim 50\text{K}$, so the magnetic resistivity essentially coincides with the raw resistivity at lower temperatures). A small kink arises in $\rho_{\text{mag}}^{\text{exp}}(T)$ at $T = 3.3\text{K}$, reflecting the transition from paramagnetic phase I to phase II [22, 26] mentioned above. The experimental resistivity is seen to exhibit the classic 'shape' for a strongly correlated HF metal, increasing from zero at $T = 0$ and going through a coherence peak at $T = 4\text{K}$, before decreasing through a small log-linear regime (similar to that shown in figure 6(a) of I) to a shallow minimum at $T = 375\text{K}$; increasing thereafter at higher temperatures where it shows conventional metallic behaviour.

To compare $\rho_{\text{mag}}^{\text{exp}}(T)$ to theory, first recall from I that the asymptotic scaling resistivity $\rho_{\text{mag}}(T)$ is a universal function of $T = !_L$ for fixed c and β (being independent of the local interaction U and hybridization V); see e.g. figure 8 of I. For a chosen $(c; \beta)$ the scaling $\rho_{\text{mag}}(T)$ is then straightforwardly superposed onto $\rho_{\text{mag}}^{\text{exp}}(T)$ with an appropriate rescaling of the temperature and resistivity axes, thus enabling the low-energy scale $!_L$ to be determined. The asymptotic scaling $\rho_{\text{mag}}(T)$ is shown in figure 1 (dotted line) for a moderate $c = 0.5$ and $\beta = 0$, with the resultant coherence scale thereby found to be $!_L = 5.5\text{K}$. It is seen to capture the experimental resistivity up to $T = 100\text{K}$, but above this it deviates below experiment, continuing as it must to decrease monotonically (see figure 8 of I) and hence lacking the minimum occurring experimentally for CeB₆ at $T_{\text{min}} = 375\text{K}$, i.e. $T_{\text{min}} = T_{\text{min}} = !_L = 5.5\text{K}$.

As discussed in I (figure 8 inset), the latter behaviour is physically natural and

readily encompassed theoretically. No real HF material is in the universal scaling regime 'for ever' – it must be exited sooner or later with increasing T . Deviation of $\rho_{\text{mag}}(T)$ from its asymptotic scaling form at sufficiently high temperatures signifies the onset of non-universality; and the location of the non-universal minimum in $\rho_{\text{mag}}(T)$ provides an opportunity to identify the ratio $U=V^2$ of effective bare material parameters, which will be helpful in making a prediction for the ω -dependence of the optical conductivity $\sigma(\omega; T)$. Specifically, for the chosen $\epsilon_c = 0.5$; $\epsilon = 0$, we find that the theoretical $\rho_{\text{mag}}(T)$ indeed has a minimum at $T_{\text{min}} \approx 70$ (as in experiment) for $U=V^2 \approx 12$. This is illustrated in figure 1, where we show the resultant theoretical $\rho_{\text{mag}}(T)$ for $U = 4.75$; $V^2 = 0.4$ (solid curve) and $U = 2.45$; $V^2 = 0.2$ (dashed curve). The two $\rho_{\text{mag}}(T)$'s barely differ from the asymptotic scaling resistivity for $T \gg 100\text{ K}$, are essentially coincident with each other across the entire T -range, and each possesses a weak minimum at $T \approx 375\text{ K}$. Except naturally for a small neighbourhood around the low-temperature phase transitions (which the theory does not seek to address), the resultant theoretical $\rho_{\text{mag}}(T)$ is seen to be in rather good agreement with experiment, as evident further from the inset to figure 1 where the corresponding d.c. conductivity $\sigma_{\text{mag}}(T)$ is shown. A CEF excitation is known to occur at 2.5 meV (30 K) [27] (with a second lying at a much higher energy, 46 meV [27]); but as judged from the above comparison this appears to play a minor role in the d.c. transport itself.

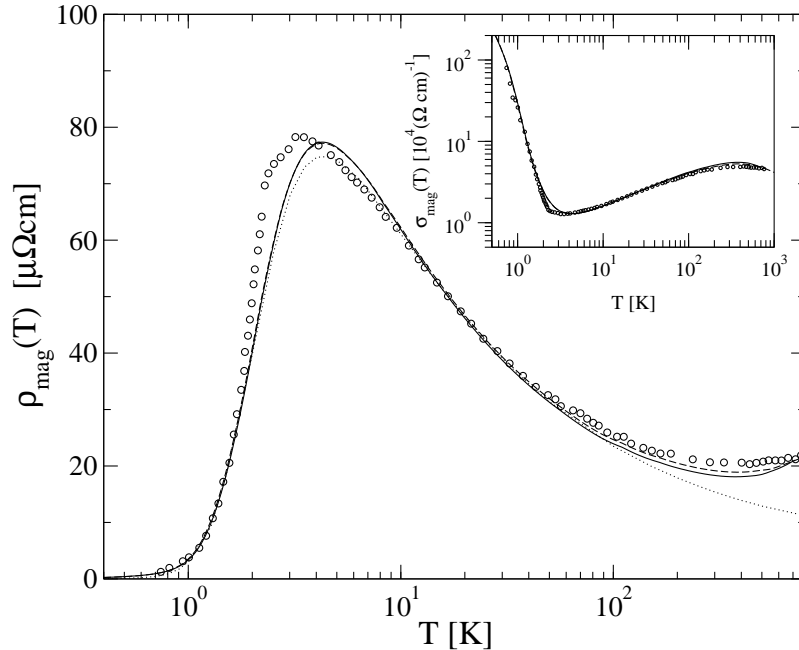


Figure 1. Comparison of experimental $\rho_{\text{mag}}^{\text{exp}}(T)$ (circles) for CeB_6 [22] to theory, on a log-linear scale. The solid curve shows $\rho_{\text{mag}}(T)$ for $U = 4.75$; $V^2 = 0.4$, while the dashed curve is for $U = 2.45$; $V^2 = 0.2$; both theory sets have common $\epsilon_c = 0.5$; $\epsilon = 0$ and the same $\epsilon_L = 5.5\text{ K}$. The dotted curve shows the asymptotic scaling resistivity. Inset: the d.c. conductivity $\sigma_{\text{mag}}(T) = 1/\rho_{\text{mag}}(T)$ on a log-log scale.

To determine the optical conductivity on all ω -scales, including non-universal

frequencies, requires U and V^2 to be separately specified as discussed in I. That is clearly not provided by the above analysis, but a reasoned prediction for $(\epsilon'; T)$ may nonetheless be made. For fixed $U=V^2 \approx 12$ as above, we find that varying U across the range $2.5 \leq U \leq 5$ produces only a modest change in both the ϵ' - and T -dependence of $(\epsilon'; T)$, leading in particular to a direct gap absorption lying in the interval $200 \leq \omega \leq 300 \text{ cm}^{-1}$; as well as a quasiparticle weight Z on the order of 10^{-2} that is consistent with the effective mass $(m^* = m_e) m \approx 100$ deduced from the specific heat coefficient $\gamma = 250 \text{ mJ mol}^{-1} \text{ K}^{-2}$ measured for Phase-I of CeB_6 [22,26]. In other words, on the assumption that the reasonably wide U -range above encompasses the behaviour of CeB_6 , the optics are relatively insensitive to the precise value of U .

To that end we show in figure 2 the predicted optical conductivity for $U = 2.45$, $V^2 = 0.2$, with the $\epsilon' = \epsilon'_L$ -dependence of the theoretical $(\epsilon'; T)$ converted to ϵ' in cm^{-1} using $\epsilon'_L = 5.5K$ ($\approx 3.8 \text{ cm}^{-1}$) deduced from the above analysis of the d.c. resistivity; and with $(\epsilon'; T)$ shown for a range of temperatures from $1.1K$ to $660K$. As $\epsilon' \rightarrow 0$, the T -dependence of the dynamical conductivity follows the d.c. values shown in the inset to figure 1. At the lowest temperature $T = 1.1K \approx \epsilon'_L = 5$ an emergent low-frequency Drude absorption on frequency scales $\omega \leq 1 \text{ cm}^{-1}$ is evident in $(\epsilon'; T)$ (see also figure 9 of I), separated by a clear optical pseudogap centred on $\omega \approx 10 \text{ cm}^{-1}$ from a strong direct gap absorption centred on $\omega \approx 250 \text{ cm}^{-1}$. The Drude absorption is rapidly suppressed on increasing T , being all but dead by $T \approx \epsilon'_L = 5.5K$; while the optical pseudogap is progressively 'filled in' on temperature scales set by ϵ'_L . The direct gap absorption is largely unaffected by temperature until $T \approx (5-10)\epsilon'_L$ or so; but is significantly eroded by $T \approx 110K$ and in essence destroyed by room temperature.

The optical conductivity of CeB_6 has in fact been measured by Kimura et al [23], but only in the frequency interval $50 \text{ meV} \approx 400 \text{ cm}^{-1}$ to $10 \text{ eV} \approx 8 \times 10^4 \text{ cm}^{-1}$, and at a temperature of $300K$. No strong direct gap absorption was observed, itself suggesting that the absorption occurs at frequencies on the order of $\omega \approx 200 \text{ cm}^{-1} \approx 300K$ or less; instead a broad, featureless and monotonically decreasing spectral lineshape was found. This is of course consistent with the prediction from figure 2 above that the direct gap peak is almost completely washed away at room temperature. In order to observe non-trivial ϵ' - and T -dependence in the optical conductivity of CeB_6 , we thus suggest the frequency domain be extended down to $\omega \approx 10 \text{ cm}^{-1}$ (or lower to observe the Drude absorption), and that experiments be performed at considerably lower temperatures such as those shown in figure 2.

4. YbAl₃

Our main focus in I and [13] has been the strongly correlated heavy fermion regime where the f -level $\epsilon_f \approx 0$ lies well below the Fermi level, with $\epsilon_f + U \approx 0$ well above it, such that the f -electrons are essentially localized, $n_f \approx 1$. The underlying local moment approach is not however restricted to the Kondo lattice regime, and in particular can

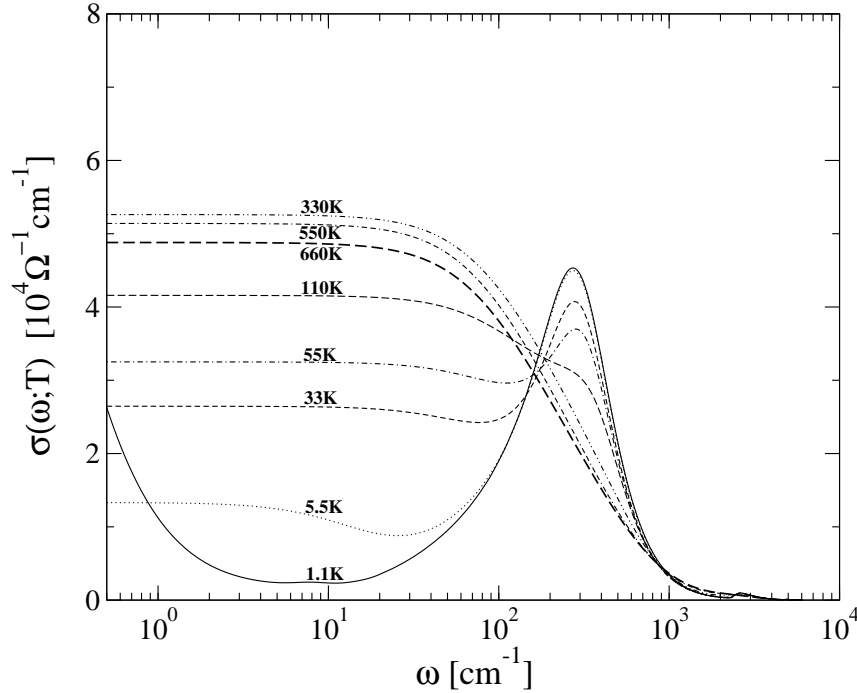


Figure 2. Predicted optical conductivity of CeB_6 : $\sigma(\omega; T)$ vs. ω in cm^{-1} at temperatures $T = 1.1\text{K}; 5.5\text{K}; 33\text{K}; 55\text{K}; 110\text{K}; 330\text{K}; 550\text{K}$ and 660K .

also readily handle intermediate valence (IV) behaviour. In this case, depletion for example of n_f from unity reflects the fact that ϵ_f lies relatively close to the Fermi level, such that the appropriate $\epsilon = 1 + 2\epsilon_f = U$ regime is $\epsilon = 1$.

The compound YbAl_3 , which crystallizes in a simple cubic Cu_3Au -type structure and does not order magnetically [28], provides a prime example of IV behaviour. Figure 3 shows the experimental d.c. resistivity of YbAl_3 , and its non-magnetic homologue LuAl_3 , at ambient pressure (data from [28] with the tiny residual resistivity subtracted). The resultant magnetic resistivity $\rho_{\text{mag}}^{\text{exp}}(T)$ is also shown in Figure 3, obtained simply by subtracting the resistivity of LuAl_3 from that of YbAl_3 (the samples [28] are high quality single crystals, hence the factor a in equation (2.1) is taken as unity). $\rho_{\text{mag}}^{\text{exp}}(T)$ is seen to increase monotonically with T , lacking the coherence peak seen in strongly correlated HF materials. This behaviour is characteristic of IV [29], as too is e.g. the low/moderate effective mass in the range $m^* = 1.5 - 3.0$ inferred from dHvA [30], optical [31] and specific heat [32] measurements; and the Yb mean valence $z_v = 2 + n_f$ is estimated experimentally as $z_v = 2.65 - 2.8$ [32,33].

In the strongly correlated HF regime, physical properties such as $\rho_{\text{mag}}(T)$ exhibit scaling as a function of $T = T_L$, independent of the interaction U and hybridization V as detailed in I; occurring formally for all $T = T_L$ in the asymptotic strong coupling limit, and in material practice over a significant albeit naturally finite $T = T_L$ range as seen above for CeB_6 (and in [15] for Kondo insulators). This is not by contrast the case in the IV regime, and neither is it to be expected. Here the 'full set' of bare/material parameters $\epsilon_f; \epsilon; U$ and V must be specified. To compare theory to experiment for YbAl_3

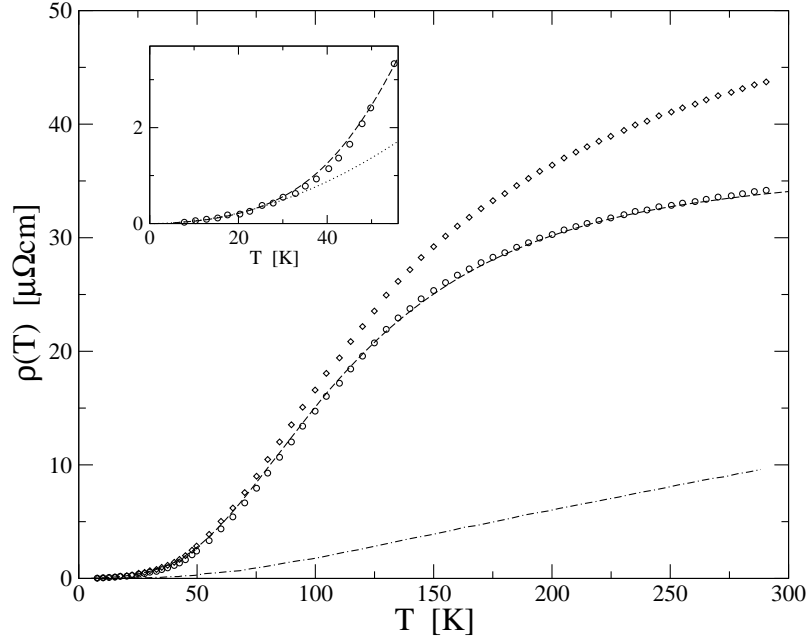


Figure 3. The d.c. resistivity of YbAl_3 (diamonds) and LuAl_3 (point-dash line), from [28] with the small residual resistivity subtracted. The experimental $\rho_{\text{mag}}^{\text{exp}}(T)$ (circles) is obtained by subtracting $\rho(T) - \rho(0)$ for LuAl_3 from that for YbAl_3 . The theoretical $\rho_{\text{mag}}(T)$ (dashed line) is obtained for $c = 0.5$; $\mu = 1.2$; $U = 4.9$; $V^2 = 0.8$, and superimposed on $\rho_{\text{mag}}^{\text{exp}}(T)$ with $T_L = 254\text{K}$. The level of agreement between theory and experiment is clear. Inset: the low temperature behaviour; including (dotted line) a fit to the asymptotic Fermi liquid form $\rho_{\text{mag}}(T) / T^2$, which is seen to persist in both experiment and theory up to $T = 30\text{K}$.

we consider a moderate $c = 0.5$ with $\mu = 1.2$; $U = 4.9$ and $V^2 = 0.8$; corresponding to a modest interaction strength $U = \epsilon_0 = 1.4$ (with $\epsilon_0 = V^2 \epsilon_0(c)$ as in I) and an $\epsilon_f = 0.49$ close to the Fermi level ($\epsilon_f = \epsilon_0 = 0.44$). The resultant f-band filling is found to be $n_f \approx 0.65$ ($z_v \approx 2.65$), consistent with the mixed valence nature of YbAl_3 ; and a quasiparticle weight $Z \approx 0.05$ is found, implying an effective mass $m^* \approx 20$ that is likewise consistent with experiment as above.

The theoretical d.c. resistivity $\rho_{\text{mag}}(T)$ vs. $T = T_L$ for these parameters has been determined, and superposed onto the experimental $\rho_{\text{mag}}^{\text{exp}}(T)$ in the usual way. The resultant low-energy scale is found thereby to be $T_L = 254\text{K}$, and comparison between theory and experiment is shown in figure 3. The agreement is clearly excellent, for all temperatures. The inset to figure 3 shows the low temperature behaviour on an expanded scale, together with a fit (dotted line) to the $T \rightarrow 0$ Fermi liquid form $\rho_{\text{mag}}(T) / T^2$. As known from experiment [32], and seen also in the present theory, this asymptotic form is seen to persist up to a temperature $T_{FL} \approx 30\text{K}$ that is an order of magnitude lower than $T_L = 254\text{K}$; and about which fact we make two brief comments. First, to emphasise that this arises naturally here within a theoretical approach to the periodic Anderson model itself (with no appeal e.g. to calculations based upon a single-impurity Anderson model [32]). Second, the quantitative distinction between T_{FL} and

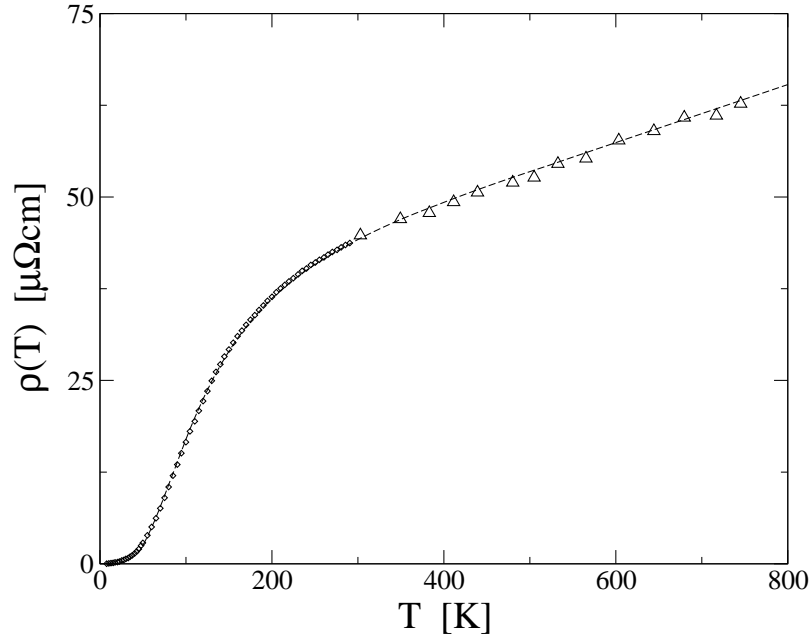


Figure 4. Theoretical $\rho(T)$ for YbAl_3 (dashed line) up to 800K, compared to the experimental results of [28] (diamonds) up to $T = 300\text{K}$ and of [34] from 300–750K (triangles), as detailed in text.

ρ_L is in our view to be anticipated; for ρ_L is the natural low-energy scale in the problem, and since $\rho(T)/T^2$ is the asymptotic $T \rightarrow 0$ behaviour, we would as such expect it to arise only for $T \rightarrow \rho_L$.

While the experimental data shown in figure 3 extend up to $T \approx 300\text{K}$, the theoretical $\rho_{\text{mag}}(T)$ may be used to predict the full $\rho(T)$ for YbAl_3 over a much larger temperature interval. To that end we simply calculate $\rho_{\text{mag}}(T)$ at higher T , and add to it the resistivity of LuAl_3 representing the phonon contribution, itself extended to higher T by linear extrapolation of the Lu data in figure 3 (point-dash line, and which extrapolation is clearly warranted). The resultant $\rho(T)$ is shown in figure 4 out to $T = 800\text{K}$; and we note that it continues to increase monotonically above 300K, precluding as such the occurrence of a coherence maximum at a T in excess of that shown in figure 3. Experimental results for $\rho(T)$ up to $T \approx 750\text{K}$ have in fact been reported [34]. This data does not appear to be quite as clean as that of [28] in the interval $50\text{K} < T < 300\text{K}$, but for $T > 50\text{K}$ the $\rho(T)$ from [34] collapses very well onto that of [28] (considered above) with an overall y -axis rescaling factor $a = 1.2$ (equation (2.1)). Taking this a , the resultant $\rho(T)$ from [34] is shown in figure 4 in the temperature interval 300–750K; and is seen to agree well with the theoretical result.

We turn now to the optical conductivity of YbAl_3 , which has only recently been measured at infrared frequencies and below [31]. This is reproduced in the top panel of figure 5, from which three key features are evident [31]: the low-frequency Drude response characteristic of the free carriers; a depleted pseudogap occurring at low temperatures (at $\hbar\omega \approx 20\text{meV}$) and flanked on its right by a shoulder at $\hbar\omega \approx 50\text{--}60\text{meV}$;

followed by the broad, strong direct gap (or mid-infrared, mIR) peak centred near $\omega \approx 250$ meV.

Coverlet

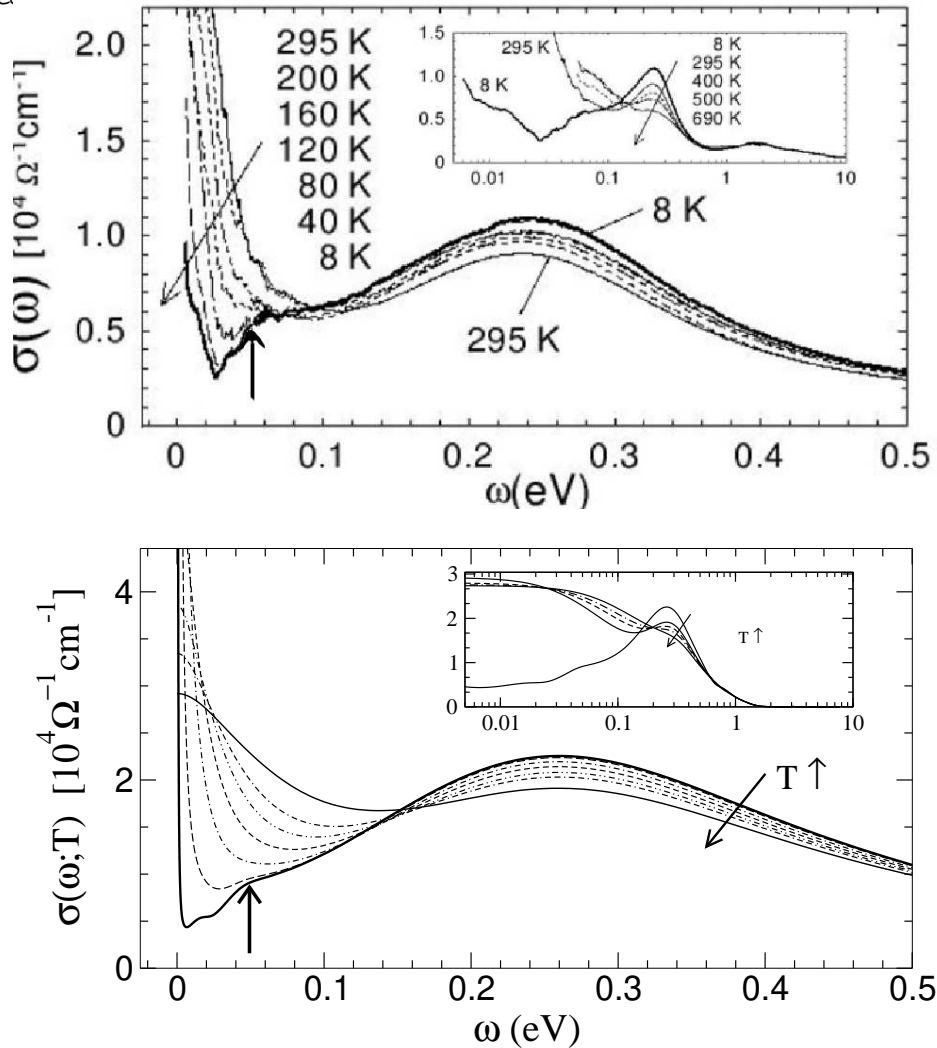


Figure 5. Top panel: experimental optical conductivity of YbAl_3 [31]. Bottom panel: theoretical $\sigma(\omega; T)$ for the same parameters as in Figure 3; at the same temperatures and on the same frequency scale as in experiment. The vertical arrow in both panels indicates the position of the theoretically predicted shoulder, at $\omega \approx 2\Delta_L \approx 50$ meV. The insets show the thermalevolution of $\sigma(\omega; T)$ for higher temperatures. The overall experimental lineshape including the pseudogap, shoulder and mIR peak, as well as their thermalevolution, is well reproduced by theory.

The bottom panel in Figure 5 shows the theoretical optical conductivity at the same temperatures and on the same frequency scale as experiment, obtained using the same bare parameters employed in Figures 3, 4, and with $\Delta_L = 254$ K as deduced above; in other words with no additional input other than that inferred from the d.c. transport comparison. Barring a mismatch in the relative intensity of the direct gap peak on which we comment below, the agreement between theory and experiment is seen to be rather good in terms of the pseudogap structure, the shoulder, the position and width

of the mIR peak, and the thermal evolution of the optical conductivity. The shoulder in particular merits comment, being a distinct spectral feature that is thermally destroyed with increasing temperature [31]. It has been speculated in [31] (not unreasonably) that its origin may lie outside the scope of the PAM and/or be material specific. The present results however suggest to the contrary. Theoretically, we find that the existence of the shoulder shown in figure 5 is not specific to the particular set of bare material parameters considered, but rather characteristic of IV in general terms – a clear optical shoulder arising in the vicinity of $\omega' \approx 2\omega_L$ as the bare parameters are varied over quite a significant range. Its origins reflect the underlying behaviour of the f-electron self-energy, and we do not therefore have a simple physical explanation for it; but neither do we doubt its generic occurrence. For the case of YbAl_3 , with $\omega_L \approx 250\text{K}$ deduced from d.c. transport as above, the shoulder thus lies at $\omega \approx 50\text{meV}$ as indicated by the vertical arrows in figure 5 and agreeing rather well with experiment.

Finally, we comment on the mismatch in the vertical (intensity) axes in figure 5. The theoretical $(\sigma'; T)$ represents of course the conductivity in the absence of phonons, which inevitably introduces a certain mismatch between theory and experiment as $\sigma' \rightarrow 0$ at temperatures high enough for the phonons to kick in; but the phonon background would not extend up to mIR frequencies, so the intensity of the direct gap peak in theory and experiment should agree. The fact that it does not could obviously mean that a different bare parameter set may be more appropriate than that identified here. Alternatively, the issue may be experimental. The $(\sigma'; T)$ spectra are obtained [31] via Kramers-Kronig transformation of the total reflectance between 7meV and 35eV, with a Hagen-Rubens formula used for low-energy extrapolation; and with several different spectral sources employed in different frequency intervals, which require matching using appropriate constant factors (see e.g. [35]). This is intricate, and there is undoubtedly the possibility of error in determining the absolute intensity of the direct gap. A surface impedance probe such as the one used in [35] might be able to resolve the matter; while if the issue is not experimental then a more extensive scan of the bare parameter space is required. That notwithstanding, however, the present theory does appear to provide a remarkably consistent description of both transport and optics in YbAl_3 .

5. CeAl_3

The classic system CeAl_3 has long been subject to extensive investigation, see e.g. [1, 35(42)]. In contrast to its Yb cousin considered above, CeAl_3 is a prototypical heavy fermion material; as attested for example by the large specific heat coefficient $1.4 \times 10^4 \text{mJmol}^{-1}\text{K}^{-2}$ [39] and corresponding effective mass $m^* \approx 700$ [35, 39].

A helpful starting point for comparison of theory to experiment is a rough knowledge of the parameter regime to which the system belongs. In the case of CeAl_3 we can glean such information from the unusual behaviour of the experimental optical conductivity [35], which is shown in the top panel of figure 7 below. Typical features

found in optical line shapes of HF systems are the Drude peak at low frequencies, followed by a pseudogap, with a strong direct gap (or m IR) absorption at higher frequencies (see e.g. figures 2,5,10). In the case of CeAl₃ however, while the Drude peak is clearly evident at low T, a distinct pseudogap and the m IR peak are absent. In fact there is little frequency dependence beyond the Drude absorption range.

From our theoretical work in I we know that increasing ρ_c , and hence reducing the conduction band filling n_c , acts to diminish the pseudogap (see inset to figure 10 of I); relatedly, it also tends to suppress the direct gap absorption, suggesting that a suitably large ρ_c is required for CeAl₃. However this by itself is not sufficient: a large ρ_c , but with a modest hybridization V between the f-levels and the conduction band, can still give rise to a distinct m IR absorption. A suitably large hybridization thus also seems necessary to suppress strongly the direct gap absorption. Unusually large CEF parameters found in inelastic neutron scattering experiments have in fact also been attributed to a large hybridization V [40], supporting this inference. And from the large effective mass mentioned above, we know the system is in the strong correlated Kondo lattice regime, requiring a significant interaction strength U .

The picture of CeAl₃ thus suggested is of a system with low conduction band filling n_c (large ρ_c), a significant hybridization V , and strong local interactions. We have investigated this regime in some detail, and for comparison to transport and optical experiments on CeAl₃ will consider explicitly the following material parameters: $\rho_c = 1.5$ and $\alpha = 0$ (results are quite insensitive to α in the Kondo lattice regime), together with $V^2 = 1.4$ and $U = 6.9$ (or $U = \rho_0 \approx 8.4$ implying strong correlations, where $\rho_0 = V^2/\rho_c$) as in I). Additional specification of U and V^2 is of course required in order to consider the optical conductivity on all frequency scales, whereas ρ_c and α alone suffice to determine the d.c. resistivity in the scaling regime. With these parameters we find a quasiparticle weight $Z \approx 1.6 \times 10^{-3}$ and hence an effective mass $m^* \approx 625$, in good agreement with $m^* \approx 690$ deduced from specific heat measurements [35,39]. The resultant conduction band filling is $n_c = 0.17$; while the f-level occupancy $n_f = 1.0$, consistent with the formally trivalent ($z_v = 4$) nature of the Ce ion expected in the HF regime.

We first consider d.c. transport measurements. These have been obtained by several groups [35,37{39,41}], which we find in general concur well on subtraction of appropriate residual resistivities (so $\alpha = 1$ is taken in equation (2.1)). We choose to compare explicitly to the $\rho(T)$ data of [37], which is shown in figure 6 (squares) at ambient pressure with the residual resistivity subtracted out; together with the corresponding $\rho_{mag}^{exp}(T)$ (circles) obtained by further subtracting the resistivity of LaAl₃. Figure 6 also shows corresponding results for $\rho_{mag}^{exp}(T)$ obtained at a pressure $P = 0.4$ GPa [38] (triangles), using the same sample as in [37]. The theoretical $\rho_{mag}(T)$ is calculated and scaled onto the ambient pressure $\rho_{mag}^{exp}(T)$ in the usual way, leading thereby to a coherence scale of $T_L \approx 33$ K. From figure 6, comparison between theory and experiment is seen to be good up to $T \approx 45$ K, beyond which the experimental $\rho_{mag}^{exp}(T)$ drops much more rapidly with further increasing T . This is natural, for inelastic neutron scattering

Cover letter: 24.09.2010, 10:46:00, 10.10.2010, 10:46:00, 10.10.2010, 10:46:00

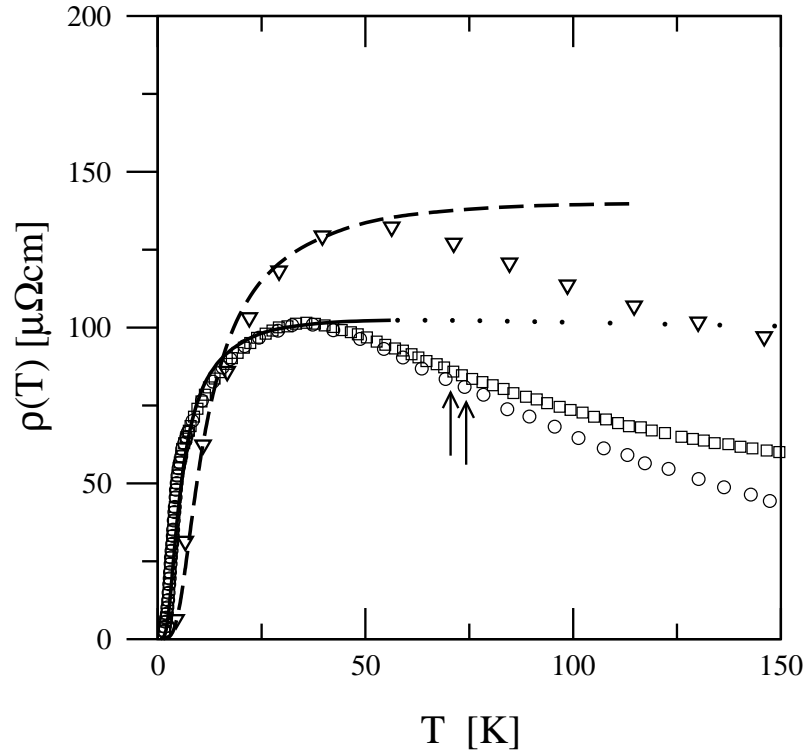


Figure 6. d.c. resistivity of CeAl_3 at ambient pressure (squares, from [37] with the residual resistivity subtracted); and the corresponding magnetic resistivity $\rho_{\text{mag}}^{\text{exp}}(T)$ (circles) [37]. The theoretical $\rho_{\text{mag}}(T)$ for $\epsilon_c = 1.5$, $\epsilon = 0$ is shown by the solid/dotted line, the resultant coherence scale being $T_L = 33\text{K}$. The agreement between theory and experiment is good for $T \leq 45\text{K}$, beyond which deviations naturally occur due to the presence of two crystal field split levels at 6.1m eV (71K) and 6.4m eV (75K) [40], marked by arrows. Triangles denote $\rho_{\text{mag}}^{\text{exp}}(T)$ for CeAl_3 at a higher pressure $P = 0.4\text{ GPa}$ [38]. The dashed line shows the same theoretical curve as used for comparison to the ambient pressure data, but with simple rescaling of the axes, leading to $T_L(P = 0.4\text{ GPa}) = 71\text{K}$.

experiments [40] show two higher crystal field levels occurring at almost the same energy, 6.1m eV (70.8K) and 6.4m eV (74.2K) above the ground state. Marked in Figure 6, these are accessed thermally as T approaches 70K , and provided they couple effectively to the conduction band (as appears to be the case here) the two additional conduction channels diminish the resistivity significantly.

We now comment briefly on the high pressure magnetic resistivity shown in Figure 6. The coherence scale $T_L = ZV^2$ itself naturally varies with pressure, but in the strongly correlated Kondo lattice regime the T -dependence of the magnetic resistivity should depend universally on T/T_L alone (x2). The same theoretical $\rho_{\text{mag}}(T)$ employed for comparison to the ambient pressure data should thus, with mere rescaling of the axes, account for $\rho_{\text{mag}}^{\text{exp}}(T)$ at $P = 0.4\text{ GPa}$ (again up to the temperature at which the CEF excitations kick in). That indeed it does is shown in Figure 6 (dashed line); the resultant coherence scale being found to be $T_L(P = 0.4\text{ GPa}) = 71\text{K}$.

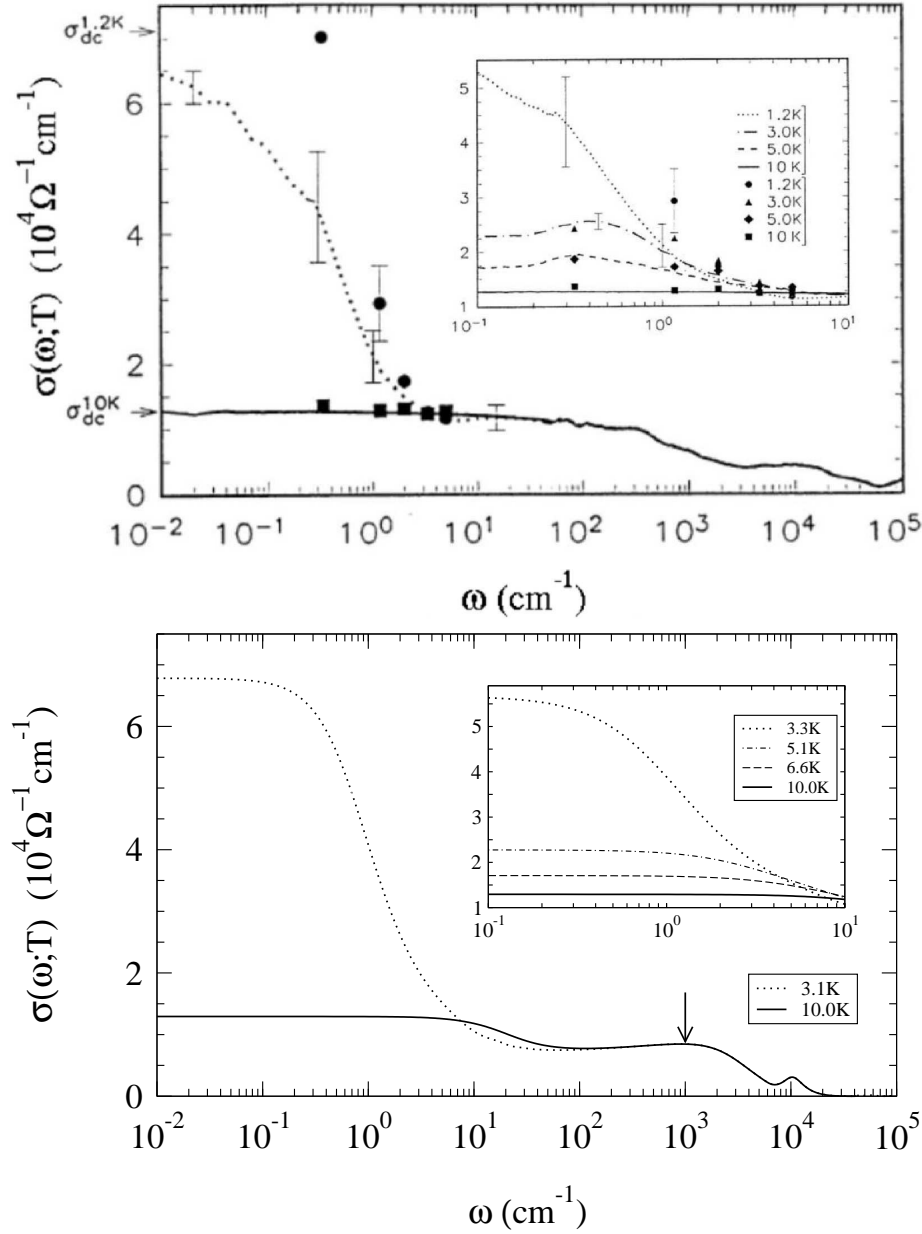


Figure 7. Top panel: experimental optical conductivity of CeAl_3 at the temperatures indicated, from [35]. Bottom panel: theoretical $\sigma(\omega; T)$. Discussion in text. The vertical arrow denotes the location of the direct gap, where a mid-IR peak is usually found for other HF systems.

Finally we turn to the optical conductivity, the experimental results [35] shown in figure 7 (top panel) being obtained from reflectance spectroscopy (lines) and surface impedance measurements (points). The bottom panel shows the theoretical $\sigma(\omega; T)$ obtained with the bare parameters specified above, converted to cm^{-1} using $\hbar\omega_L = 33\text{K}$ inferred above from static transport. The theory evidently captures the unusual optical characteristics of CeAl_3 , and agreement with experiment is seen to be rather good. A strong Drude peak, and a very shallow pseudogap, are seen at the lowest temperatures

in theory and experiment; the Drude absorption collapsing on a temperature scale of 10K, above which very little T dependence is found across the entire frequency range. Most significantly, no distinct direct gap/IR peak arises, the spectrum being largely featureless (the small feature visible at 10^4 cm^{-1} in the theoretical ($!;T$) occurs on the effective bandwidth scale, and its intensity diminishes further with increasing U). The nominal location of the direct gap itself can however be determined theoretically from the renormalized band structure underlying the present theory (as considered in I, see figure 11). It is found to lie at $! \sim 10^3 \text{ cm}^{-1}$ as marked in figure 7, albeit that no sharp absorption occurs in its vicinity.

6. CeCoIn₅

This recently discovered [43], moderately heavy fermion compound crystallizes in a tetragonal structure consisting of alternate layers of CeIn₃ and CoIn₂. It superconducts below $T_c \approx 2.3 \text{ K}$ (the highest transition temperature of all known HF systems at ambient pressure [43]), and is paramagnetic for $T > T_c$. The experimental resistivities

(T) determined by four different groups [43-46] are shown in figure 8. That they differ widely presumably reflects intrinsic difficulties in measuring the dimensions of relatively small samples. Their basic equivalence is however seen by taking the results of one as a reference and rescaling the y-axis for each of the remaining data sets. With this, as shown in the inset to figure 8, all four resistivities collapse to essentially common form (that of [46] deviating just slightly at higher T). These differences are nonetheless potentially significant when comparing to theory, for which the magnetic contribution $\rho_{\text{mag}}^{\text{exp}}(T)$ is required, obtained as in equation (2.1) by subtracting the resistivity of the non-magnetic LaCoIn₅. The results in figure 8 show that the a factor in equation (2.1) | the relative weight of (T) compared to that for the non-magnetic homologue | could vary by a factor of up to four or so, and is not therefore known with confidence.

Figure 9 shows the experimental $\rho_{\text{mag}}^{\text{exp}}(T)$ (open circles) determined in [44] by subtracting the resistivity of LaCoIn₅ from that for CeCoIn₅; corresponding as such to $a = 1$ (or equivalently, if e.g. (T) from [45] had been used instead, to an a of ~ 2). To compare to theory we consider the parameters $\nu_c = 0.5$ and $\nu_s = 0$, with $U = 3.75$ and $V^2 = 0.8$ (corresponding to an intermediate coupling strength $U = \nu_c \nu_s \approx 1$). The resultant theoretical $\rho_{\text{mag}}(T)$ is compared to experiment in figure 9 (solid line), yielding a coherence scale of $T_L = 60 \text{ K}$. It matches $\rho_{\text{mag}}^{\text{exp}}(T)$ for $15 \text{ K} \lesssim T \lesssim 100 \text{ K}$, the deviation at low temperatures presumably reflecting the approach to the superconducting state. The deviation above $T \approx 100 \text{ K}$ also appears natural, since a direct determination of the CEF energy level scheme from inelastic neutron scattering [47] shows an excited level at 8.6 meV or $\sim 100 \text{ K}$ (with a second at a much higher energy, 24.4 meV), the extra conduction channel acting to diminish $\rho_{\text{mag}}^{\text{exp}}(T)$ more rapidly than the 1-channel theory.

Our guess is that the latter inference is correct, at least qualitatively. A degree of caution is however required, since this is sensitive to a change in the value of a . To

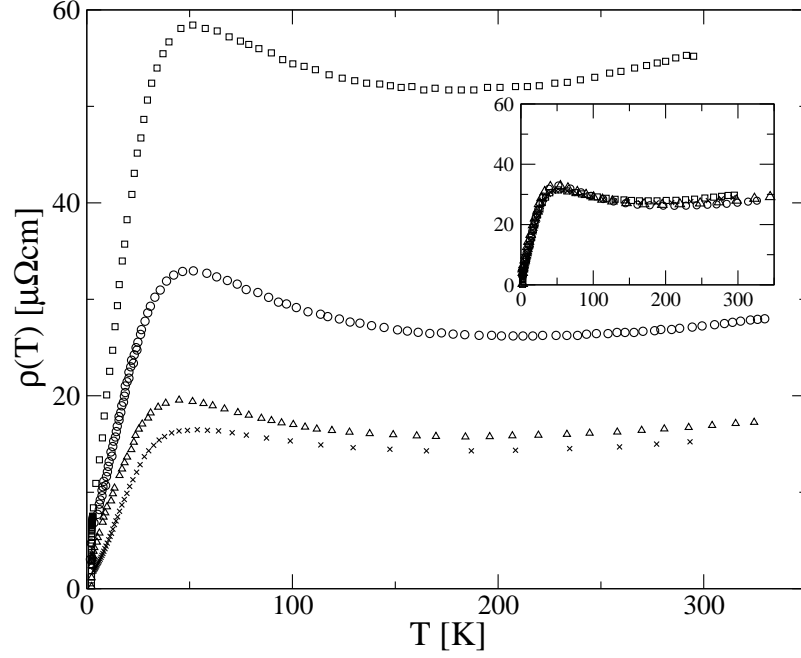


Figure 8. Experimental resistivity of CeCoIn_5 measured by different groups: Ref [44] (circles), Ref [46] (squares), Ref [43] (triangles) and Ref [45] (crosses). Inset: showing collapse of experimental resistivities to common form on rescaling the y-axis alone.

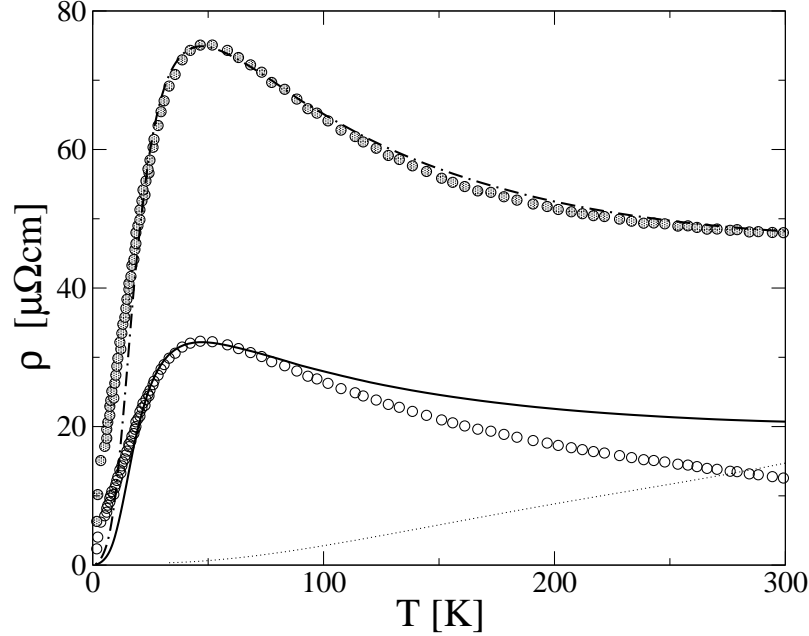


Figure 9. CeCoIn_5 . Open circles denote the experimental $\sigma_{\text{mag}}^{\text{exp}}(T)$ from [44], corresponding to $a = 1$ in equation (2.1) (dotted line shows the resistivity of LaCoIn_5). The solid line shows the theoretical $\sigma_{\text{mag}}(T)$ for the bare parameters described in text, with coherence scale $\xi_L = 60\text{K}$. Filled circles denote an experimental $\sigma_{\text{mag}}^{\text{exp}}(T)$ obtained with $a = 2/3$ instead; the corresponding theoretical $\sigma_{\text{mag}}(T)$ (again with $\xi_L = 60\text{K}$) is now shown as a point-dash line. Full discussion in text.

illustrate that, figure 9 also shows a new $\rho_{\text{mag}}^{\text{exp}}(T)$ (filled circles) obtained with $a = 2/3$ in equation (2.1). The theoretical $\rho_{\text{mag}}(T)$ with the same coherence scale $\hbar_L = 60\text{K}$, but with the overall y-axis naturally increased by factor of $2/3$, now describes $\rho_{\text{mag}}^{\text{exp}}(T)$ very well for essentially all $T \leq 15\text{K}$. The quantitative influence of the extra conduction channel can thus be assessed with confidence only if the relative values of the resistivity for the magnetic and non-magnetic compounds are known accurately; although we add that the inferred low temperature coherence scale $\hbar_L = 60\text{K}$ is not itself sensitive to a .

We turn now to the optical conductivity. Experimental results from reflectivity measurements [45] are shown in figure 10 (top panel), with the ω -dependence on a log scale up to $\omega = 30\text{cm}^{-1}$ and a linear scale thereafter (separated by a vertical line). For $\omega < 30\text{cm}^{-1}$ the results are extrapolated (dashed lines) towards the d.c. limit [45], as required for the Kramer-Kronig analysis of the reflectivity that leads to the experimental $\rho(\omega; T)$ shown. The theoretical $\rho(\omega; T)$ is shown in the lower panel, for the bare parameters specified above, with $\hbar_L = 60\text{K}$.

The comparison between theory and experiment is at least qualitatively satisfactory, albeit not as good as for YbAl_3 or CeAl_3 (perhaps unsurprisingly given the quasi-2D nature of CeCoIn_5). The pseudogap at $T = 10\text{K}$ is seen to lie at $\omega \approx 65\text{cm}^{-1}$, and as in experiment shifts gradually to higher ω with increasing temperature and fills up progressively on the scale of $\omega \approx 2\hbar_L$ or $60 \rightarrow 120\text{K}$. The direct gap absorption in theory and experiment lies at $\omega_{\text{dir}} \approx 600\text{cm}^{-1}$; and starts to lose spectral weight significantly for $T \gtrsim 50\text{K}$ or so, i.e. on the scale of \hbar_L itself. This suggests that CeCoIn_5 is not in the strong coupling, Kondo lattice regime; since in strong coupling the direct gap/IR absorption is significantly eroded for temperatures approaching the order of the direct gap itself ($\approx 600\text{cm}^{-1}$ or 900K in the present case), see e.g. figure 12 of I. For CeCoIn_5 by contrast, significant thermal erosion is seen to occur for $T \gtrsim 50\text{K}$ with $\omega_{\text{dir}} \approx 20$, which behaviour is typical of intermediate coupling strengths. That also appears consistent with dHvA measurements [48], which yield a moderate effective mass m^* in the range $10 \rightarrow 20$.

Two further points should be mentioned. First, the $\omega \lesssim 30\text{cm}^{-1}$ values of the theoretical $\rho(\omega; T)$ are clearly lower than the experimental extrapolations. As $\omega \rightarrow 0$, the latter extrapolate to the d.c. conductivity obtained in [45]. The d.c. limit of the theoretical $\rho(0; T)$ by contrast gives the $\rho_{\text{mag}}(T)$ shown in figure 9 (solid line), and aside from the $T = 292\text{K}$ case this agrees well with the experimental d.c. conductivity of [44] — which as seen from figure 8 differs by a factor of two or so from that of [45]. The issue here appears largely to be experimental, reflecting the significant difference between the resistivities of [44] and [45]. Second, the vertical arrows at $\omega \approx 250\text{cm}^{-1}$ in the experimental $\rho(\omega; T)$ of figure 10 indicate weak additional absorption that has been ascribed [45] to a Holstein band due to coupling to a bosonic mode. This is not of course included in the present theory, which thus shows somewhat less absorption in the region.

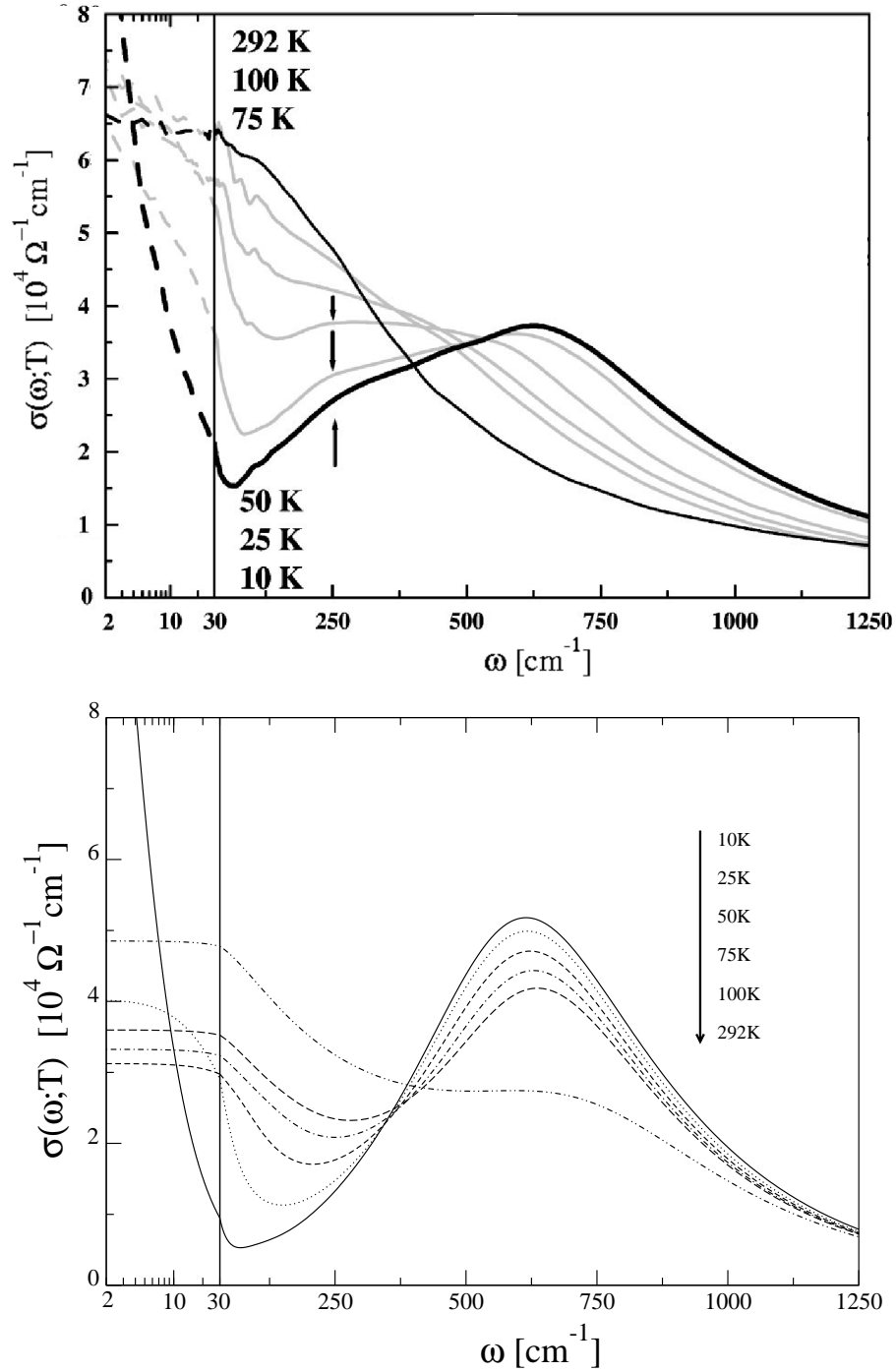


Figure 10. Top panel: experimental optical conductivity of CeCoIn_5 at various temperatures [45]. Bottom panel: corresponding theoretical ($!; T$) obtained for the parameter set $c = 0.5$; $= 0$, $U = 3.75$ and $V^2 = 0.8$, with $!_L = 60 \text{ K}$ (42 cm^{-1}). In both cases the frequency axis is logarithmic up to $! = 30 \text{ cm}^{-1}$ and linear thereafter (separated by a vertical line). Full discussion in text.

7. Conclusion

We have here employed a local moment approach to the periodic Anderson lattice developed in I, to make direct comparison to d.c. transport and optical conductivities of

CeB_6 , YbAl_3 , CeAl_3 and CeCoIn_5 . The Yb compound is a representative intermediate valence material, and the others typify heavy fermion behaviour, from the strongly correlated Kondo lattice regime appropriate to CeAl_3 and CeB_6 to what we believe is the somewhat weaker coupling case of CeCoIn_5 . In broad terms more or less all characteristic features of the optics and transport of these materials are captured; the natural exception, omitted from the model itself, being crystal field effects which may (or may not) show up in the experimental resistivity as a reduction below 1-channel behaviour at suitably high temperatures. The theory in general performs rather well quantitatively, and also captures notable features specific to individual systems – for example the existence of a low-frequency shoulder observed in the optics of YbAl_3 [31], or the absence of any significant direct gap/m IR absorption in CeAl_3 [35].

Minimalist though it is the underlying model, and theory for it, thus appear to provide quite a comprehensive and successful description of experiment. This we attribute in no small part both to the dominance of the local electron scattering inherent to the model itself, and the need to provide an adequate theoretical description of such on all experimentally relevant frequency and temperature scales.

Acknowledgments

We are grateful to the following for permission to quote their experimental results: L Degiorgi, H Okamura, G Oomi and F. Steglich. We express our thanks to the EPSRC for supporting this research.

References

- [1] Grewe N and Steglich F 1991 Handbook on the Physics and Chemistry of Rare Earths vol 14 ed K A Gschneider Jr. and L L Eyring (Amsterdam: Elsevier) p 343
- [2] Hewson A C 1993 The Kondo Problem to Heavy Fermions (Cambridge: Cambridge University Press)
- [3] Aeppli G and Fisk Z 1992 Comm. Condens. Matter Phys. 16 155
- [4] Fisk Z et al 1996 Physica B 223–224 409
- [5] Takabatake T et al 1998 J. Magn. Magn. Mater. 177–181 277
- [6] Degiorgi L 1999 Rev. Mod. Phys. 71 687
- [7] Riseborough P S 2000 Adv. Phys. 49 257
- [8] Vollhardt D 1993 Correlated Electron Systems vol 9 ed V J Emery (Singapore: World Scientific)
- [9] Puschke T, Jarrell M and Freericks J K 1995 Adv. Phys. 44 187
- [10] Georges A, Kotliar G, Krauth W and Rozenberg M 1996 Rev. Mod. Phys. 68 13
- [11] Gebhard F 1997 The Mott Metal-Insulator Transition (Springer Tracts in Modern Physics) vol 137 (Berlin: Springer)
- [12] Logan D E and Vidhyadhiraja N S 2005 J. Phys.: Condens. Matter 17 2935–2958
- [13] Vidhyadhiraja N S and Logan D E 2004 Eur. Phys. J. B 39 313–334
- [14] Smith V E, Logan D E and Krishnamurthy H R 2003 Eur. Phys. J. B 32 49
- [15] Vidhyadhiraja N S, Smith V E, Logan D E and Krishnamurthy H R 2003 J. Phys.: Condens. Matter 15 4045–4087
- [16] Strong S P and Millis A J 1994 Phys. Rev. B 50 12611
- [17] Kashiba S, Makiawa S, Takahashi S and Tachiki M 1986 J. Phys. Soc. Jpn. 55 1341

- [18] Cornut B and Coqblin B 1972 Phys. Rev. B 5 4541
- [19] Yamada K, Yosida K and Hanzawa K 1984 Prog. Theor. Phys. 71 450
- [20] Suzuki H, Kitazawa H, Naka T, Tang J and Kido G 1998 Sol. St. Comm. 107 447
- [21] Gorshunov B, Sluchanko N, Volkov A, Dressel M, Knebel G, Loidl A and Kuni S 1999 Phys. Rev. B 59 1808
- [22] Sato N, Sumiyama A, Kuni S, Nagano H and Kasuya T 1985 J. Phys. Soc. Jpn. 54 1923-1932
- [23] Kimura S, Nanba T, Kuni S and Kasuya T 1994 Phys. Rev. B 50 1406
- [24] Nakamura S, Goto T and Kuni S 1995 J. Phys. Soc. Jpn. 64 3941-3945
- [25] Goodrich R G et al 2004 Phys. Rev. B 69 054415
- [26] Maroenat C, Jaccard D, Sierro J, Flouquet J, Onuki Y, Komatsubara T 1990 J. Low Temp. Phys. 78 261
- [27] Zimigib1E et al 1984 Phys. Rev. B 30 4052
- [28] Ohara S, Chen G F and Sakamoto I 2001 J. Alloys. Comps. 323-324 632-635
- [29] Schweitzer H and Czycholl G 1991 Phys. Rev. Lett. 67 3724
- [30] Ebihara T et al 2000 J. Phys. Soc. Jpn. 69 895
- [31] Okamura H, Michizawa T, Nanba T and Ebihara T 2004 J. Phys. Soc. Jpn. 73 2045
- [32] Cornelius A L et al 2002 Phys. Rev. Lett. 88 117201
- [33] Suga S et al 2002 Abstr. Fall Meet., Physical Society of Japan, 7aXC-6.
- [34] Rowe D M, Kuznetsov V L, Kuznetsova L A and Ming 2002 J. Phys. D : Appl. Phys. 35 2183-2186
- [35] Awasthi A M, Degiorgi L, Guner G, Dalichaouch Y and Maple M B 1993 Phys. Rev. B 48 10692
- [36] Rieborough P S 2003 Phys. Rev. B 67 045102
- [37] Kagaya T, Munakata K and Oomi G 1993 J. Alloys and Compounds 192 239-241
- [38] Oomi G and Kagaya T 1996 J. Phys. Soc. Jpn. 65 2732-2733
- [39] Andres K, Graebner J E and Ott H R 1975 Phys. Rev. Lett. 35 1779
- [40] Gorenchkin E A, Osborn R and Sashin I L 1999 J. Appl. Phys. 85 6046
- [41] Jaccard D, Chin R and Sierro J 1988 Helv. Phys. Acta 61 530-537
- [42] Jaccard D and Flouquet J 1985 J. Magn. Mater. 47& 48 45-50
- [43] Petrovic et al 2001 J. Phys.: Condens. Matter 13 L337-L342
- [44] Nakatsuji S et al 2002 Phys. Rev. Lett. 89 106402
- [45] Singley E J, Basov D N, Bauer E D and Maple M B 2002 Phys. Rev. B 65 161101
- [46] Nicklas M et al 2001 J. Phys.: Condens. Matter 13 L905-L912
- [47] Bauer E D et al 2004 J. Appl. Phys. 95 7201
- [48] Hall D et al 2001 Phys. Rev. B 64 212508